This is a repository copy of *Understanding Iodine Chemistry Over the Northern and Equatorial Indian Ocean*.

White Rose Research Online URL for this paper:
https://eprints.whiterose.ac.uk/150493/

Version: Published Version

Article:
Mahajan, Anoop S., Tinel, Liselotte orcid.org/0000-0003-1742-2755, Sarkar, Amit et al. (6 more authors) (2019) Understanding Iodine Chemistry Over the Northern and Equatorial Indian Ocean. Journal of Geophysical Research: Biogeosciences. pp. 8104-8118. ISSN 2169-8961

https://doi.org/10.1029/2018JD029063

Reuse
Items deposited in White Rose Research Online are protected by copyright, with all rights reserved unless indicated otherwise. They may be downloaded and/or printed for private study, or other acts as permitted by national copyright laws. The publisher or other rights holders may allow further reproduction and re-use of the full text version. This is indicated by the licence information on the White Rose Research Online record for the item.

Takedown
If you consider content in White Rose Research Online to be in breach of UK law, please notify us by emailing eprints@whiterose.ac.uk including the URL of the record and the reason for the withdrawal request.

eprints@whiterose.ac.uk
https://eprints.whiterose.ac.uk/

JGR Atmospheres

RESEARCH ARTICLE
10.1029/2018JD029063

Understanding Iodine Chemistry Over the Northern and Equatorial Indian Ocean

Anoop S. Mahajan[1], Liselotte Tinel[2], Amit Sarkar[3], Rosie Chance[2], Lucy J. Carpenter[2], Shrivardhan Hulswar[4], Prithviraj Mali[1], Satya Prakash[5], and P. N. Vinayachandran[6]

[1]Centre for Climate Change Research, Indian Institute of Tropical Meteorology, Pune, India, [2]Wolfson Atmospheric Chemistry Laboratories, Department of Chemistry, University of York, York, UK, [3]National Centre for Antarctic and Ocean Research, Goa, India, [4]Department of Marine Sciences, Goa University, Goa, India, [5]Indian National Centre for Ocean Information Services, Hyderabad, India, [6]Indian Institute of Sciences, Bangalore, India

Key Points:
- NO_x titration buffers atmospheric concentrations of iodine oxide
- Fluxes of inorganic iodine determine iodine oxide levels outside elevated NO_x regions
- A strong gradient in iodine chemistry is observed from close to the coast toward the remote ocean environment

Supporting Information:
- Supporting Information S1
- Figure S1
- Figure S2
- Figure S3

Correspondence to:
A. S. Mahajan,
anoop@tropmet.res.in

Citation:
Mahajan, A. S., Tinel, L., Sarkar, A., Chance, R., Carpenter, L. J., Hulswar, S., et al. (2019). Understanding iodine chemistry over the northern and equatorial Indian Ocean. *Journal of Geophysical Research: Atmospheres*, *124*, 8104–8118. https://doi.org/10.1029/2018JD029063

Received 29 MAY 2018
Accepted 10 FEB 2019
Accepted article online 15 FEB 2019
Published online 18 JUL 2019

Author Contributions:
Conceptualization: Anoop S. Mahajan
Data curation: Anoop S. Mahajan
Formal analysis: Anoop S. Mahajan
Methodology: Anoop S. Mahajan
Project administration: Anoop S. Mahajan
Supervision: Anoop S. Mahajan
Visualization: Anoop S. Mahajan
Writing - original draft: Anoop S. Mahajan
Writing – review & editing: Anoop S. Mahajan

©2019. American Geophysical Union. All Rights Reserved.

Abstract Observations of halogen oxides, ozone, meteorological parameters, and physical and biogeochemical water column measurements were made in the Indian Ocean and its marine boundary layer as a part of the Second International Indian Ocean Expedition (IIOE-2). The expedition took place on board the oceanographic research vessel *Sagar Nidhi* during 4–22 December 2015 from Goa, India, to Port Louis, Mauritius. Observations of mixed layer depth, averaged temperature, salinity, and nitrate concentrations were used to calculate predicted iodide concentrations in the seawater. The inorganic iodine ocean-atmosphere flux (hypoiodous acid [HOI] and molecular iodine [I_2]) was computed using the predicted iodide concentrations, measured atmospheric ozone, and wind speed. Iodine oxide (IO) mixing ratios peaked at 0.47 ± 0.29 pptv (parts per trillion by volume) in the remote open ocean environment. The estimated iodide concentrations and HOI and I_2 fluxes peaked at 200/500 nM, 410/680 nmol·m^{-2}·day^{-1}, and 20/80 nmol·m^{-2}·day^{-1}, respectively, depending on the parameterization used. The calculated fluxes for HOI and I_2 were higher closer to the Indian subcontinent; however, atmospheric IO was only observed above the detection limit in the remote open ocean environment. We use NO_2 observations to show that titration of IO by NO_2 is the main reason for this result. These observations show that inorganic iodine fluxes and atmospheric IO show similar trends in the Indian Ocean marine boundary layer, but the impact of inorganic iodine emissions on iodine chemistry is buffered in elevated NO_x environments, even though the estimated oceanic iodine fluxes are higher.

1. Introduction

Reactive halogen species (chlorine, bromine, and iodine) have been shown to play an important role in the chemistry of the lower troposphere. They lead to the depletion of ozone (O_3), change the oxidizing capacity of the atmosphere through hydrogen and nitrogen oxides, lead to oxidation of toxic metals such as mercury, and, in the case of iodine, cause formation of new particles in the marine environment (Saiz-Lopez & von Glasow, 2012). Historically, halogen oxides in the lower troposphere attracted attention mainly in the polar environment where elevated concentrations (>10 parts per trillion by volume [pptv] equivalent to pmol/mol) were observed during the springtime and led to near total depletion of O_3 and elemental mercury (e.g., Frieß et al., 2001; Hausmann & Platt, 1994; McConnell et al., 1992; Saiz-Lopez, Chance, et al., 2007; Schroeder et al., 1998).

Of the different halogen compounds, iodine species have the most significant impact on ozone in the global troposphere (Carpenter, 2003; Saiz-Lopez & von Glasow, 2012; Saiz-Lopez, Plane, et al., 2012). Early studies speculated on the role of oceanic emissions of iodine compounds on atmospheric chemistry, with some laboratory-based experiments suggesting an ocean to atmosphere flux (Chameides & Davis, 1980; Garland & Curtis, 1981; Liss & Slater, 1974; Miyake & Tsunogai, 1963). A major source for organic volatile iodine species (e.g., CH_3I and CH_2I_2) is biogenic production by microalgae and macroalgae (Alicke et al., 1999; Carpenter, 2003; O'Dowd et al., 2002; Saiz-Lopez & Plane, 2004). Inorganic iodine species, notably I_2 and hypoiodous acid (HOI), are mainly formed through heterogeneous surface reactions of iodide, present in the surface waters, and gas phase ozone (Carpenter & Nightingale, 2015). This process can be described by reactions (R1) and (R2), both of which occur in different steps (Hayase et al., 2010; Sakamoto et al., 2009) leading to the release of photochemically reactive iodine species in the marine atmosphere.

$$I^- + O_3 + H^+ \rightarrow HOI + O_2 \quad (R1)$$

$$HOI + I^- + H^+ \leftrightarrow I_2 + H_2O \quad (R2)$$

The inorganic iodine species are the largest source of iodine in the marine atmosphere where they form a significant sink for atmospheric ozone through reaction (R1) and through catalytic destruction of ozone in the atmosphere (Carpenter et al., 2013; Ganzeveld, 2009; Mahajan et al., 2012).

The detection of iodine monoxide (IO) at the coastal atmospheric laboratory at Mace Head (Alicke et al., 1999) triggered further work on the exact role of iodine emissions. Subsequent studies showed that significant biogenic iodine emissions from macroalgae can lead to new particle formation at coastal sites (Jimenez, 2003; Mahajan et al., 2009; McFiggans et al., 2004, 2010; O'Dowd et al., 2002, 2004; Saiz-Lopez et al., 2006). Ground-based observations (Frieß et al., 2001; Saiz-Lopez, Mahajan, et al., 2007; Mahajan, Shaw, et al., 2010) followed by satellite measurements (Saiz-Lopez, Chance, et al., 2007; Schönhardt et al., 2008) confirmed the importance of iodine chemistry in the polar troposphere, with iodine playing a major role in modulating the oxidation capacity of the Antarctic boundary layer. Outside the polar environment, the first observations of IO were made at Mace Head (Alicke et al., 1999) followed by Cape Grim, Tasmania, and later at the Canary Islands, showing peak IO concentrations of 6, 2.2, and 4 pptv, respectively (Allan et al., 2000), although some influence of coastal macroalgae emissions was detected. More recent observations at Cape Verde showed year-round presence of IO at about 1.5 pptv, with little annual variability (Read et al., 2008; Mahajan, Plane, et al., 2010). Since these island-based campaigns, ship-based studies have also confirmed the presence of IO in the remote marine boundary layer (MBL), although at lower mixing ratios typically below 1 pptv (Commane et al., 2011; Großmann et al., 2013; Hepach et al., 2016; Mahajan et al., 2012; Prados-Roman et al., 2015). Observations of IO above instrumental detection limits have also been made in the free troposphere, highlighting the importance of iodine chemistry above the MBL (Dix et al., 2013; Puentedura et al., 2002). For a complete list of measurements of iodine compounds in the MBL, please refer to the published review (Saiz-Lopez & von Glasow, 2012).

Modeling studies have shown the significant impact that iodine can have on the atmosphere even at low concentrations (Saiz-Lopez, Lamarque, et al., 2012; Saiz-Lopez et al., 2014; Sherwen, Schmidt, et al., 2016, Sherwen, Evans, et al., 2016). According to model estimates, a large geographical variation in the IO mixing ratios in the MBL is expected, with higher concentrations observed in the tropics and extratropics (Prados-Roman et al., 2015; Sherwen, Evans, et al., 2016). The gradient is mainly driven by the emission strength of inorganic source gases (HOI and I_2), which are in turn driven by the rate of ozone deposition and the iodide content in the seawater (Carpenter et al., 2013; Chance et al., 2014; MacDonald et al., 2014). Indeed, in the Indian Ocean, the model predicts a large gradient in IO, with higher concentrations close to the equator where higher ozone concentrations and sea surface temperature (SST) are observed (Prados-Roman et al., 2015; Saiz-Lopez et al., 2014). But apart from a cruise in the Southern Indian Ocean (Prados-Roman et al., 2015) and ground-based observations at Maldives (Oetjen, 2009), there are no other reported observations of IO in this region hitherto.

The North Indian Ocean and its neighboring continents are characterized by their unique climatic conditions due to strong monsoonal winds (Burkill et al., 1993). The southwest monsoon, which determines the intensity of rainfall over the Indian subcontinent, is a function of ocean-atmospheric interaction and is teleconnected with warming physical processes like El Niño and the Indian Ocean Dipole. In response to this forcing, the upper ocean circulation and hydrography show strong variability (Kumar et al., 2006; Saji et al., 1999). The Northern Indian Ocean also harbors different distinct biogeochemical regimes (Dileepkumar, 2006). The western and eastern Indian oceans (mainly Arabian Sea and Bay of Bengal) are fairly biologically productive compared with the equatorial Indian Ocean. Since the first International Indian Ocean Expedition (IIOE; https://scor-int.org/project/iioe-1), our understanding of the biogeochemistry of this region has increased considerably (Wiggert et al., 2009). Recent studies reveal that the equatorial Indian Ocean has been warming for more than a century, at a rate faster than any other region in the tropical oceans. The summer SST in the central east Indian Ocean warm pool has increased by 0.7 °C, and the western Indian Ocean has seen a warming of 1.2 °C compared with those during preindustrial times (Roxy et al., 2014). A major question is whether the biogeochemistry in the Indian Ocean has been altered significantly by this raise in temperature. To help answer this, a research campaign named the Second International

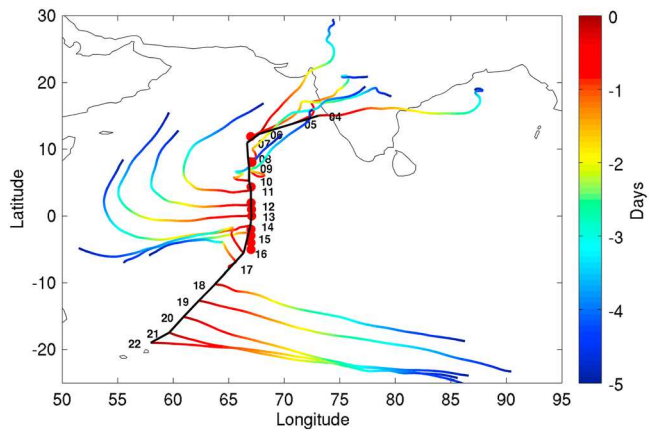

Figure 1. The Second International Indian Ocean Expedition cruise track along with the HYbrid Single-Particle Lagrangian Integrated Trajectory (HYSPLIT)-calculated 5-day backtrajectories arriving at noon local time on every day of the cruise. The day of December 2015 is written next to the trajectory arrival point. The sampling locations where measurements of oceanic parameters were made are highlighted as red circles along the track.

Indian Ocean Expedition (IIOE-2) was conducted in the Indian Ocean to study extensively the ocean physics, chemistry, and biology. The study area was similar to the first IIOE that was carried out on board research vessel *Anton Bruun* during May–June 1963, almost 50 years ago. As a part of IIOE-2, we report observations of IO in the equatorial Indian Ocean, during a cruise in December 2015 along a track from India to Mauritius. We also estimate the iodide levels in the seawater based on the nutrient concentrations, salinity, and SST (Chance et al., 2014) and thereby compute the flux of inorganic iodine species to the atmosphere. We compare spatial trends in the measured atmospheric iodine concentrations with those of the ocean-air fluxes and explore differences in the context of the atmospheric chemistry of iodine.

2. Observation and Methodology

2.1. Atmospheric Parameters

The study was conducted on board the oceanographic research vessel *Sagar Nidhi* as a part of IIOE-2 in December 2015. The expedition started at Goa, India, on 4 December 2015 and finished in Mauritius on 22 December 2015. Figure 1 shows the track of the ship and the 5-day backtrajectories arriving at noon on every day of the cruise calculated using the HYbrid Single-Particle Lagrangian Integrated Trajectory (HYSPLIT) model using the EDAS-40 km. (Draxler & Rolph, 2003).

Surface ozone was monitored using a U.S. Environmental Protection Agency-approved photometric UV analyzer (Ecotech EC9810B). Calibration of the O_3 analyzer was done on every fifth day using an inbuilt O_3 calibrator for instrument zero and span correction and with gas standards before and after the expedition, which showed an ~3% drift. The O_3 analyzer was placed in the same place as the indoor unit of the multi-axis differential optical absorption spectroscopy (MAX-DOAS), with an inlet close to the outdoor unit (~2-m inlet gas line).

The MAX-DOAS (Hönninger et al., 2004; Plane & Saiz-Lopez, 2006; Platt & Stutz, 2008; Wagner et al., 2004) instrument (EnviMes) was set up on the second level of the ship, pointing toward the fore looking out to the horizon. The instrument is made up of an indoor unit, housing two spectrometers with a spectral resolution of 0.7 nm (UV: 301.20–463.69 nm and Vis: 443.54–584.19 nm), and an outdoor unit, containing a scanning telescope. The outdoor unit was mounted on a mechanical gimbal table. This setup reduced the ship's pitch and roll to within ±2°. The scanner also has a high-sensitivity (±0.01°), fast-response (0.1 s) inclinometer and corrects the elevation angle actively during measurements. The true elevation angle was logged and angles within a range of 0.2° of the set elevation angles (1°, 2°, 3°, 5°, 7°, 10°, 20°, and 90°) were used for analysis. The spectra were calibrated using mercury emission lines from a mercury calibration lamp every day and with the Fraunhofer spectrum (Kurucz et al., 1984). Nonlinearity of the spectrometers was also corrected in addition to the offset and dark current, which were collected on each day. Spectra were collected at each angle for 1 s, resulting in a full scan every 12 s including motor movement time. The data were then averaged for 1 hr to improve the signal-to-noise ratio. The QDOAS software was used for the retrieval of slant columns from the spectra (Fayt & Van Roozendael, 2013). The cross sections used for IO retrieval in the 415-t 440-nm spectral window were: IO (Gómez Martín et al., 2005), NO_2 220 K and 298 K (Vandaele et al., 1997), H_2O (Rothman et al., 2013), O_4 (Greenblatt et al., 1990), O_3 (Bogumil et al., 2003), glyoxal (Volkamer et al., 2005), a ring spectrum (Chance & Spurr, 1997), a second Ring spectrum following Wagner et al. (2009), a liquid water spectrum (Pope & Fry, 1997), a stray light-correction offset, and a third-order polynomial. Sensitivity of the analysis to wavelength windows and included cross sections has been done in the past (Gómez Martín et al., 2016; Mahajan et al., 2012) and is not included here. The error estimation follows the same procedure as reported before (Mahajan et al., 2012; Prados-Roman, 2015). The cross section of water is not well quantified in the spectral range of IO and hence could lead to some errors in the retrieval (Lampel et al., 2015); however, we avoid the largest water bands in order to reduce these errors. It should be noted that the liquid water cross section has a low spectral resolution and hence can have a small effect on

the retrieved trace gas column densities. However, these have also been tested rigorously in the past by our group (Mahajan et al., 2012; Prados-Roman., 2015) and other groups around the world (Dinter et al., 2015; Peters et al., 2014; Sadeghi et al., 2012; Vountas et al., 2007), and the above mentioned analysis setting has been used in most open ocean MAX-DOAS observations of IO. Großmann et al. (2013) have discussed in detail the impact of liquid water and its potential influence on trace gas retrievals and found that in their data set the influence was almost negligible, which is also expected here. The residual root mean square in the IO region was between 2.5×10^{-4} and 5×10^{-4}, resulting in 2σ IO differential slant column densities (DSCDs) detection limits of 1.4×10^{13} to 2.8×10^{13} molecules/cm^2. NO_2 was also retrieved in this region, with a detection limit ranging between 5.3×10^{14} and 9.8×10^{14} molecules/cm^2. For the retrieval of O_4, the spectral range used was 350–386 nm, with BrO (Wilmouth et al., 1999) and HCHO (Meller & Moortgat, 2000), in addition to O_3 223 K and 243 K, NO_2 220 K and 298 K, O_4 and two Ring spectra included with a third-degree polynomial. The residual root mean square in the O_4 region was between 1.7×10^{-4} and 6×10^{-4}, resulting in 2σ O_4 DSCD detection limits of 0.7×10^{42} to 2.6×10^{42} molecules^2/cm^5. Observations of other species such as glyoxal, bromine oxide, and formaldehyde, which were also retrieved during this study, are not discussed in detail here. Surface mixing ratios were calculated from the MAX-DOAS DSCDs using the O_4 slant columns retrieved during the study by the "O_4 method" (Mahajan et al., 2012; Prados-Roman et al., 2015; Sinreich et al., 2010; Wagner et al., 2004). To obtain the effective light path length, the O_4 DSCDs at the lower-elevation angles (1–3°) were divided by the assumed O_4 mean concentration from the surface to 200 m above sea level. The height of this layer is based on the average last scattering altitude computed using different aerosol profiles. Standard MBL-based aerosol profiles were used for the computation. IO mixing ratios were then calculated by dividing trace gas DSCDs by the computed path lengths. The errors were derived from the DOAS fitting errors in the O_4 and IO DSCDs, combined with small errors in the mean O_4 extinction coefficient and the air density due to the uncertainty of the layer height. Further errors are likely to be introduced by the assumption that the IO layer has a constant mixing ratio up to the last scatter altitude and that the entire differential O_4 absorption, relative to the zenith sky viewing direction, occurs in the line-of-sight direction. Hence, the errors on the O_4 method are most likely underestimated, which is why we use 2σ errors to estimate the uncertainty on the mixing ratios. Further information on the estimation of errors on this methodology can be found in past studies where a similar methodology has been applied (Mahajan et al., 2012).

Although NO_2 DSCDs were also retrieved in the 415- to 440-nm window, they were found to be below the detection limit for most of the cruise, except close to the Indian coast. The DOAS settings used for the NO_2 analysis were similar to the IO retrieval. In order to understand the geographical distribution of NO_2 and the effect of NO_x on iodine chemistry in the Indian Ocean MBL, we also included analysis of satellite-based tropospheric NO_2 columns. We made use of three different gridded satellite tropospheric vertical column density (VCD) data sets available from the Tropospheric Emission Monitoring Internet Service (http://www.temis.nl) website. These instruments aboard the satellites are (i) the Ozone Monitoring Instrument (on board Aura, 13×24 km^2 ground pixel size) and (ii) Global Ozone Monitoring Experiment 2 (GOME-2) (on board Metop-A and Metop-B satellites, 40×80 km^2). All the satellites are Sun synchronous and equipped with spectrometers to measure the UV-visible absorption due to atmospheric NO_2. These absorption spectra are then analyzed using the DOAS technique (Platt & Stutz, 2008). Further details on the DOAS retrieval settings used for the satellite data can be found elsewhere (Boersma, 2004; Boersma et al., 2007). For NO_2, the tropospheric VCDs were calculated by subtracting the stratospheric component from the total column. We used 1° mean tropospheric NO_2 along the cruise track to study the correlation between IO and NO_2 over the course of the study.

2.2. Oceanic Parameters

Water column measurements of physical parameters were carried out at 21 stations on a meridional transect along 67°E from 12°N to 5°S (Figure 1). Profiles of temperature and salinity were obtained using the conductivity-temperature-depth system (SBE 911 plus, Sea-Bird Electronics, USA) up to a depth of 2,000 m. The accuracy for the measurements were as follows: temperature: ±0.001 °C; conductivity: ± 0.0001 S/m; and depth: ± 0.005%. The potential temperature (θ °C) was calculated based on algorithms from the international thermodynamic equation of seawater (Intergovernmental Oceanographic Commission, 2010). The mixed layer depth (MLD_{pt}) was computed based on the potential temperature difference criteria

and was considered as the depth at which potential temperature decreases by 0.5 °C compared with the surface value (Monterey & Levitus, 1997).

Of the 21 sampling stations, biogeochemical parameters were measured at 10 stations (Figure 1). Samples for nutrient analysis were collected in 250-ml narrow mouth polypropylene amber bottles (Nalgene). Each bottle was rinsed twice with the sample water prior to collection. Analysis was performed as soon as possible using a spectrometric segmented continuous flow autoanalyzer (Skalar San$^+$). The precision and accuracy for NO_3^- measurements were ± 0.06 and ±0.07 μM, respectively. Although various biogeochemical parameters were measured, we focus on the nitrate due to its strong correlation with the distribution of iodide in the global ocean (Chance et al., 2014).

As iodide concentrations in the surface water were not measured during the cruise, the following parameterizations proposed by Chance et al. (2014) were used to estimate concentrations:

$$[\text{iodide}] = 0.28\ (\pm 0.002)\times \text{SST}^2 + 1.7(\pm 0.2)\times|\text{latitude}| + 0.9(\pm 0.4)\times[\text{NO}_3^-] - 0.020(\pm 0.002)\times \text{MLD}_{\text{pt}} + 7(\pm 2)\times \text{salinity} - 309(\pm 75) \quad (1)$$

$$\ln[\text{iodide}] = 0.0026(\pm 0.0003)\times \text{SST}^2 + 0.016(\pm 0.003)\times|\text{latitude}| - 0.009(\pm 0.006)\times[\text{NO}_3^-] - 0.00044(\pm 0.00004)\times \text{MLD}_{\text{pt}} + 0.05(\pm 0.03)\times \text{salinity} + 2(\pm 1) \quad (2)$$

These parameterizations were obtained through multiple linear regression analysis of globally observed iodide concentrations in the surface seawater against the SST (°C), the absolute latitude, the MLD_{pt} (in m), nitrate concentration (μmol/L), and salinity (practical salinity unit [PSU]). Chlorophyll *a* (chl *a*) concentrations were initially also considered for the parameterization but proved to be an insignificant contributor (<5% significance level). Both parameterizations in equations (1) and (2), with R^2 of respectively 0.676 and 0.642 for the global data sets, were used to predict iodide concentrations in the surface waters of the different stations of the cruise. The uncertainty associated with these parameterizations is estimated to be between 0.5 and 2 nM (0.3–4.3%), based on error propagation using an estimation of the uncertainty of the MLD_{pt} of 5 m and neglecting the uncertainty on the latitude. This does not account for uncertainties inherent to the use of a global parameterization that has not been validated in the Indian Ocean. The predicted iodide concentrations were consequently used to calculate the fluxes of I_2 and HOI using the multiple linear regression model proposed by Carpenter et al. (2013), using the following expressions:

$$\text{flux}_{\text{I}_2} = \left[\text{O}_{3(g)}\right]*[\text{iodide}]\left[\text{O}_{3(g)}\right]*[\text{iodide}]^{1.3}*\left(1.74\times 10^9 - 6.54\times 10^8 * \ln(ws)\right) \quad (3)$$

$$\text{flux}_{\text{HOI}} = \left[O_{3(g)}\right]*\left(4.15\times 10^5 * \frac{\sqrt{\left[I^-_{(aq)}\right]}}{ws} - \frac{20.6}{ws} - 2.36\times 10^4 * \sqrt{\text{iodide}}\right] \quad (4)$$

where the fluxes are in nmol·m^{-2}·day^{-1}, [O_3] is the atmospheric ozone in nmol/mol, [iodide] in the seawater is in mol/dm^3, and the windspeed (*ws*) is in m/s. The correlation factors between the calculated fluxes using these equations and the equivalent laboratory observations were found to be 0.9991 and 0.9986, respectively (Carpenter et al., 2013). This algorithm is able to broadly capture global trends in observed iodine oxide concentrations, as has been shown recently in its successful implementation in a global model (Prados-Roman et al., 2015; Sherwen, Evans, et al., 2016, 2017). However the parameterization tends to overestimate the fluxes over seawater in low winds due to incomplete knowledge of the underlying processes (Carpenter et al., 2013; MacDonald et al., 2014; Sherwen, Evans, et al., 2016).

3. Results and Discussion

3.1. Atmospheric Parameters

Figure 2 shows variations in all the measured meteorological parameters during the cruise. The top panel shows the changes in atmospheric temperature as the ship traveled from India to Mauritius. The highest

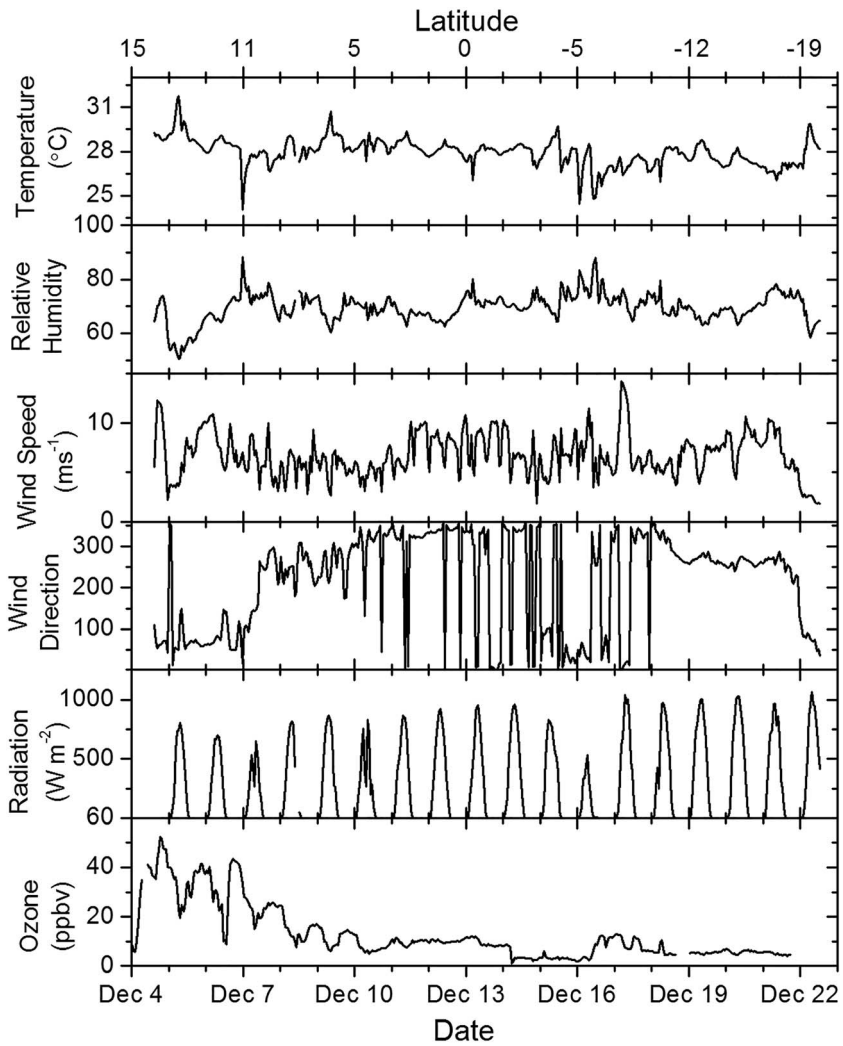

Figure 2. Data time series of the meteorological parameters and ozone mixing ratios measured over the length of the cruise.

temperature was seen away from the Indian coast, peaking at ~31.5 °C on 5 December (~12°N). Slightly lower temperatures were observed as the ship approached Mauritius, with the lowest temperature (24 °C) seen on 16 December (5 °S). The relative humidity ranged between 50% and 90% over the campaign, with typical values around 70%. The wind speed ranged between near-stagnant conditions close to Mauritius to a peak of 14.5 m/s on 17 December (7 °S). For the majority of the cruise, the wind speed ranged between 5 and 10 m/s. The wind direction close to the Indian subcontinent was northeasterly, with air masses traveling over the Indian subcontinent before arriving at the ship. The backtrajectories also indicate this (Figure 1), with the first few days of the cruise being exposed to continental air masses and hence exposed to anthropogenic emissions. Between 7 and 10 December, the wind direction changed to southwesterly, with lower influence of the Indian subcontinent. Beyond 10 December, the wind direction changed to northerly and stayed that way until 18 December, after which it wasnorth westerly until 22 December. The solar radiation (0.3 to 3 μm) varied between a minimum peak of ~500 W/m^2 on 16 December to a maximum peak of about 1,000 W/m^2 seen on several days of the study. Most of the cruise had clear-sky conditions except on 7, 10, 15, and 16 December, when long periods of overcast skies were observed. Rainfall occurred on 15 and 16 December.

The ozone mixing ratios measured during the cruise are shown in the bottom panel of Figure 2. These data have been filtered for the ship's exhaust. Elevated mixing ratios, peaking at 52 ppbv, were seen close to the Indian subcontinent on 4 December (15°N), the first day of the cruise. A large variation in the mixing ratios

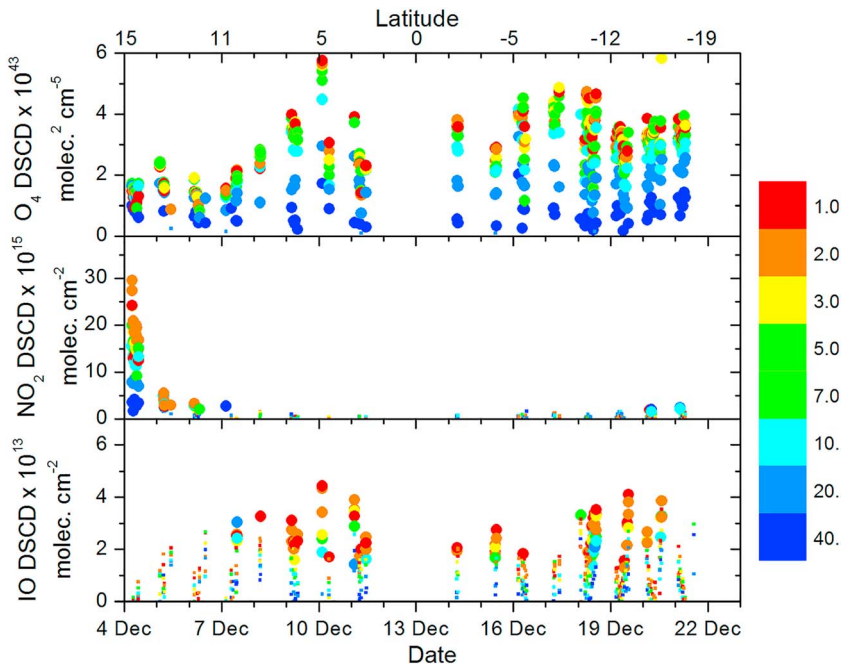

Figure 3. O_4, NO_2, and IO differential slant column densities (DSCDs) measured during the cruise. The small circles are values below the 2σ detection limit of the instrument. The different viewing elevation angles are given by the color code, shown as the color bar.

was noticed for the first few days when the air masses arriving at the ship were from the Indian subcontinent, with a diurnal variation peaking during the daytime. This diurnal pattern is indicative of photochemical production (Seinfeld & Pandis, 2006). The peak ozone mixing ratios occurred during the afternoon (between 2 and 4 p.m.). This is expected since ozone production depends on precursors, the sources of which are mainly on the subcontinent, and hence, transport of these precursors and their chemical processing to form ozone needs to be considered. The ozone levels dropped as the cruise progressed, and after 10 December (5°N), the peak values were below 20 ppbv consistently, with the absence of any clear diurnal pattern. The effect of changes in wind direction, indicating arrival of different air masses, was seen on different occasions during the cruise. For example, on 7 December, there was a sudden decrease in the ozone mixing ratios, which coincided with a change in wind direction from northeasterly winds to southwesterly. Southwesterly air masses do not pass over the Indian subcontinent, which is a source for ozone precursors, and hence, such a decrease is expected. A decrease to below 10 ppbv was seen on 15 and 16 December, which coincided with the rainfall period (Figure 2).

The MAX-DOAS DSCDs are shown in Figure 3, where the top panel shows the O_4 DSCDs, the middle panel shows the NO_2 DSCDs, and the bottom panel shows the IO DSCDs. The O_4 DSCDs can be used as a measure of the aerosol loading of the atmosphere. Over the open ocean, the O_4 DSCD values of the lowest-elevation angles are grouped together, while values of higher-elevation angles are clearly separated, which shows the existence of elevated aerosol loads close to the surface. Closer to the Indian subcontinent, most of the elevation angles are grouped together, indicating high aerosol loading with a small gradient, unlike in the open ocean environment. This is due to multiple scattering and absorption of photons by the aerosol layer. Further details about this process can be found in Platt & Stut (2008). DSCD values for NO_2 were above the detection limit only close to the Indian subcontinent, and after 7 December (~10°N) NO_2 was not observed above the detection limit of the MAX-DOAS instrument. In the case of IO, the DSCDs were below the instrumental detection limit close to the Indian subcontinent, and positive detection above the two sigma detection limit was observed only after 7 December (~10°N). The largest IO DSCDs were observed on 10 December. There was a data gap on 12 and 13 December, which was caused by instrumental problems. In general, higher values for IO were observed in the lower-elevation angles, indicating that the IO showed a decreasing vertical gradient.

Using the O_4 DSCDs, we estimated the NO_2 and IO volume mixing ratios in the boundary layer during the cruise. Mixing ratios for NO_2 were seen above the detection limit only close to the Indian subcontinent with a peak of 854 ± 223 pptv on 4 December at 11:22 a.m., 41.7° solar zenith angle. The values dropped significantly as the cruise progressed away from the subcontinent and by 7 December, NO_2 was below the detection limit. In the case of IO, the opposite trend was observed with IO mixing ratios below the detection limit close to the Indian coast. The daily averaged IO mixing ratio peaked on 9 December (~8.5°N) at 0.47 ± 0.29 pptv and then steadily reduced southward to <0.2 pptv.

The daily averaged IO mixing ratios compare well with past reports of IO in the open ocean MBL (Commane et al., 2011; Dix et al., 2013; Großmann et al., 2013; Mahajan et al., 2012; Prados-Roman et al., 2015). Values around 0.6 pptv of IO have been reported in the eastern Pacific (Mahajan et al., 2012). The largest reported database, from several cruises around the world's oceans, shows that in most of the global MBL, IO ranges between 0.4 and 1 pptv (Prados-Roman et al., 2015). Higher values have been reported in the Atlantic at the Cape Verde Atmospheric Laboratory, with a daytime IO mixing ratio of 1.5 pptv (Mahajan et al., 2009; Read et al., 2008). In the Pacific, lower IO mixing ratios were observed at the Galapagos Islands, with IO peaking at 0.9 ± 0.2 pptv (Gómez Martín et al., 2013). The current observations from the Indian Ocean are at the lower end of the range, with a maximum daytime average of 0.47 ± 0.29 pptv.

3.2. Oceanic Parameters

The latitudinal distribution of MLD_{pt} did not show any clear north-south gradient, but rather a strong variability (supporting information Figure S2). At two stations, 12°N and 10°N, the MLD_{pt} was deeper (57 and 56 m), the depth of which decreased gradually and reached its shallowest value of 11 m at 5°N. The MLD_{pt} deepened further south and reached 69 m at 1°S. Beyond that, the MLD_{pt} became shallower and at the last two sampling stations it was only 15 and 19 m at 4°S and 5°S. Mixing in the upper ocean is regulated mainly by winds, waves, incoming solar radiation, evaporation, and precipitation (Prasanna Kumar & Narvekar, 2005). The MLD_{pt} values were subsequently used to compute the iodide concentrations along the cruise transect.

The MLD_{pt}-averaged temperature distribution (supporting information Figure S3a) showed considerable latitudinal variation. At the northernmost station (12°N), the MLD_{pt}-averaged SST was 28.58 °C, which then increased by more than 1 °C at 10°N (29.68 °C). Further south, the SST reduced by 0.4 °C and remained almost constant till 4°S. At the southernmost station, the average SST reduced further and reached 28.21 °C. Interestingly, unlike SST, the MLD_{pt}-averaged salinity distribution showed a distinct north-south gradient (supporting information Figure S3b). High-salinity waters were found north of the equator (salinity >36 PSU) and gradually decreased toward the south (~35 PSU).

Variability in MLD is crucial for nutrient distribution and redistribution through turbulent mixing since it directly controls the quantity of nutrients available for phytoplankton (Mann & Lazier, 1996; D'Ortenzio et al., 2014). Deepening of the MLD facilitates injection of nutrients into the surface layer (Cullen et al., 2002). During the present study, MLD_{pt}-averaged NO_3^- also showed a distinguishable hemispheric distribution pattern (supporting information Figure S3c). North of the equator, the concentrations were fairly low (~0.5 μM) despite the moderately deep MLD_{pt} and increased in the vicinity of equatorial stations where the highest MLD_{pt} was observed. The nitrate concentrations ranged between 0.8 and 1 μM in this region. Further toward the south, the nitrate concentrations decreased to 0.7 μM, where MLD_{pt} was also shallow. Similar nutrient variations with MLD are also found in different parts of the Indian and Global Oceans like the Arabian Sea (Prasanna Kumar & Narvekar, 2005), the Bay of Bengal (Narvekar & Prasanna Kumar, 2006), the North Atlantic (Dutkiewicz et al., 2001), the North Pacific subtropical gyre (Johnson et al., 2010), and the Mediterranean Sea (D'Ortenzio et al., 2014).

Average iodide concentrations (Figure 4) were calculated for the 10 stations using the parameterization described in the previous section, using average MLD_{pt} values for all parameters. As expected, at these low latitudes (Chance et al., 2014), the calculated iodide concentrations were relatively high, ranging from 164.2 to 209.1 nM (equation (1)) and from 347 to 517 nM (equation (2)), with the higher values in the Northern Hemisphere and a dip around the equator and a gradual decrease southward toward Mauritius (Figure 4). The values estimated using equation (1) are similar to surface iodide concentrations reported for the Arabian Sea (10–22°N; 154 to 321 nM; Farrenkopf & Luther, 2002), while those estimated using

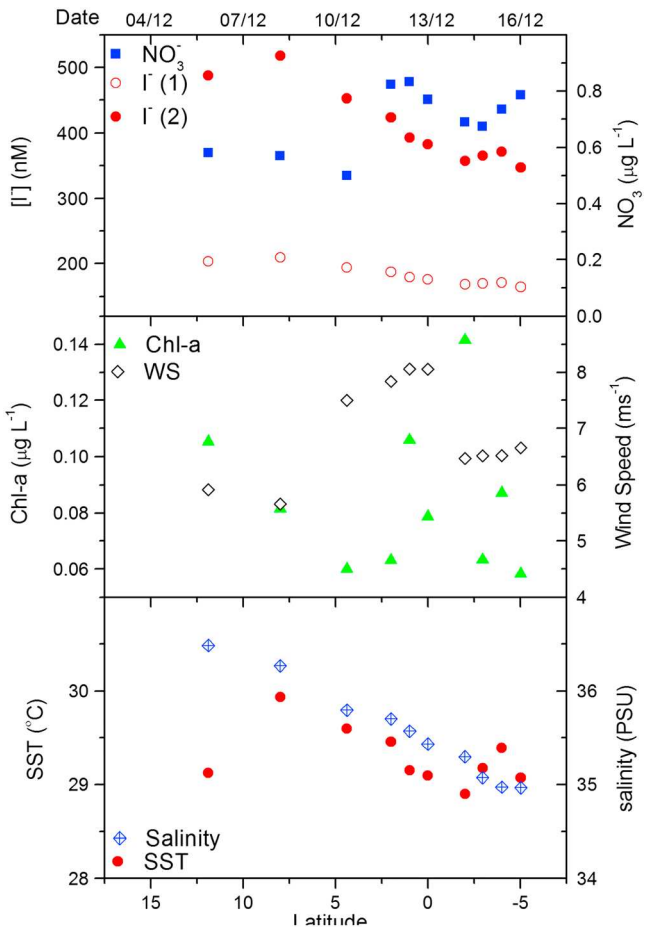

Figure 4. Observations of oceanic parameters measured during the Second International Indian Ocean Expedition and the calculated iodide concentrations are given. The bottom panel shows the sea surface temperature (SST; red circles) and the salinity (blue diamonds), the middle panel shows chlorophyll *a* (chl *a*; green triangles) and the wind speed (WS; black diamonds), and the top panel shows the nitrate concentrations (blue squares) and the iodide concentrations calculated using the two parameterizations given in equations (1) (empty red circles) and (2) (filled red circles). PSU = practical salinity unit.

equation (2) are higher. Iodate concentrations measured further south in the Indian Ocean (−4°N, 41°E, and −2°N, 43°E; Truesdale, 1978) also imply iodide concentrations of at least 166 nM, assuming a globally constant total inorganic iodine concentration of ~450 nM (Chance et al., 2014). Observed iodide concentrations at similar latitudes in the Atlantic and Pacific Oceans vary typically from 90 to 165 nM, which make the concentrations predicted using equation (2) seem unrealistically high. Indeed, of the 925 previous sea surface iodide concentrations described in Chance et al. (2014), only eight were greater than 350 nM, and only two were greater than 400 nM. Of these, all the values >400 nM were observed in coastal, sometimes brackish waters of the Skagerrak and so likely reflect very different biogeochemical conditions to the open, tropical ocean. We therefore believe that the parameterization in equation (2) does not apply well to the Indian Ocean. This view is confirmed by some very recent observations of sea surface iodide in the tropical Indian Ocean (http://doi.org/czhx). Chl *a* concentrations, given as a MLD_{pt} average for the measurement stations, are plotted in Figure 4 (middle), and the latitudinal variation suggests that it is a bad proxy for the calculated iodide ($R^2 = -0.123$), despite some similarities observed between the plots. Similar results have been obtained at the global scale, showing that chl *a* is a poor proxy for iodide distribution (Chance et al., 2014). Figures 5b and 5c show the fluxes for HOI and I_2, respectively, predicted using both calculated iodide concentrations. The wind speed (Figure 4, bottom) and ozone concentrations (Figure 5a) used in equations (3) and (4) for the calculations of the fluxes are given as daily averages for the days on which the oceanic parameters were measured. Similar to the predicted iodide concentrations, the predicted fluxes for HOI and I_2 show a very high upper value when using the iodide concentrations predicted using equation (2) (Figure 5). Previous estimates of the flux for I_2 and HOI resulted in mean annual values of, respectively, around 8×10^6 and 0.8×10^8 molecules·cm^{-2}·s^{-1} in the tropical latitudes (Sherwen, Evans, et al., 2016), which is consistent with the amount of IO observed at the Cape Verde Observatory (Carpenter et al., 2013). Großmann et al. (2013) also estimated a comparable necessary I_2 flux that was in the range of 10–22 × 10^7 molecules·cm^{-2}·s^{-1}. Here the fluxes for I_2 are estimated within the range of 1.9–18.9 × 10^6 molecules·cm^{-2}·s^{-1} (for [I$^-$] calculated using equation (1)) and 5.4–58.5 × 10^6 molecules·cm^{-2}·s^{-1} (for [I] calculated using equation (2)), and fluxes for HOI range from 68.6 to 285.9 × 10^6 molecules·cm^{-2}·s^{-1} (for [I$^-$] calculated using equation (1)) and 49.0 to 472.9 × 10^6 molecules·cm^{-2}·s^{-1} (for [I$^-$] calculated using equation (2)). The upper limits for the range calculated in this study are comparatively high, particularly using equation (2), which we believe overestimates the iodide concentration predicted in the surface waters. The high fluxes predicted are sustained by the high iodide concentrations, relatively high ozone concentrations close to the Indian subcontinent, and moderate wind speed.

The iodide concentrations predicted by equation (2) are higher by an average factor of 2.2 compared with those by equation (1). This discrepancy seems to be due to the high relative uncertainties for salinity and the last constant term of equation (2), which induce higher relative errors. The difference between both parameterizations becomes more pronounced in the calculations for the flux of molecular iodine (up to 3.25 larger) than for the flux of HOI (up to 1.6 larger) as equation (3) is more sensitive to the iodide concentration than is equation (4). The HOI flux dominates the total flux and is about 15 times larger than the I_2 flux.

3.3. Drivers of Reactive Atmospheric Iodine

Past reports have studied the relationship between different oceanic and atmospheric parameters and the atmospheric iodine content (Mahajan et al., 2012; Prados-Roman et al., 2015). In the Pacific, positive

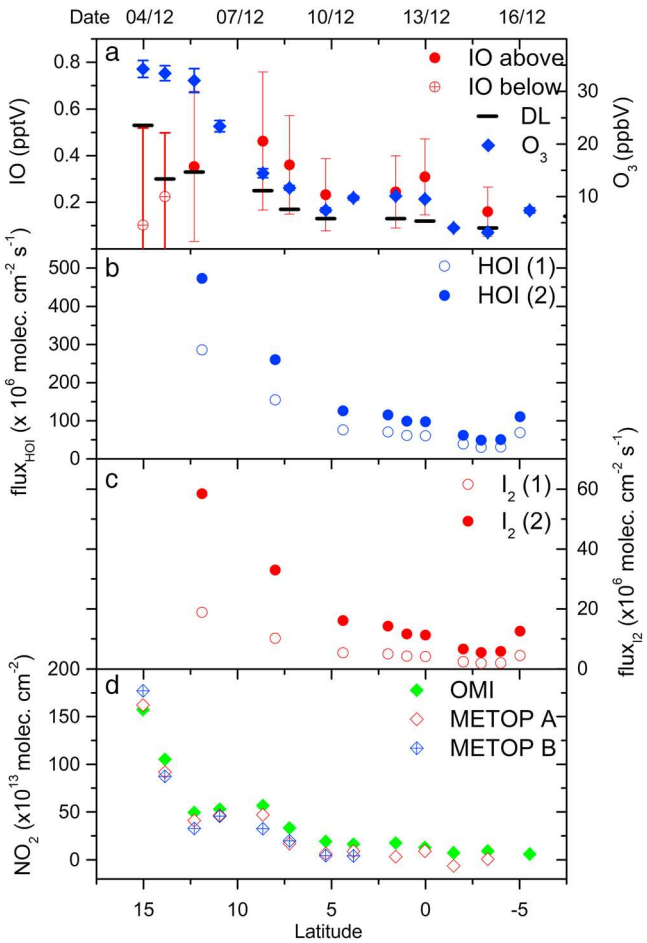

Figure 5. (a) The observed IO mixing ratios above (red circles) and below (empty red circles) the multi-axis differential optical absorption spectroscopy (MAX-DOAS) detection limit (DL; black lines) and the ozone mixing ratio (blue circles) along the cruise track. (b) Calculated ocean-atmosphere flux of hypoiodous acid (HOI) for the two parameterizations (equation (1), empty blue circles, and equation (2), filled blue circles). (c) Calculated ocean-atmosphere flux of I_2 for the two parameterizations (equation (1), empty red circles, and equation (2), filled red circles). (d) The satellite-retrieved tropospheric NO_2 vertical column densities using three satellite based instruments. OMI = Ozone Monitoring Instrument.

correlations between SST, salinity, organic iodine compound fluxes, and IO_x were reported, while O_3 and chl *a* showed significantly negative correlation. The study by Chance et al. (2014), however, did not find a significant correlation between seawater iodide content and chl *a*. During this current study, there was no significant correlation between chl *a* and the atmospheric IO concentrations, adding weight to previous reports that chl *a* concentrations are poor predictors for iodine emissions globally (Großmann et al., 2013; Mahajan et al., 2012). It should be noted that although chl *a* is a poor predictor, sea surface iodide concentrations (and hence iodine emissions) are still thought to be linked to biological productivity (Chance et al., 2014).

Figure 5 shows that although the fluxes of inorganic iodine compounds are larger closer to the Indian subcontinent, driven by higher iodide concentrations and higher ozone levels, IO is not detected above the detection limit of the instrument close to the coast. This could partially be explained by a poor parameterization for the determination of iodide concentrations in this area. Indeed, the parameterization proposed in Chance et al. (2014) has not yet been validated for the Indian Ocean. Although the calculated fluxes might thus be influenced by these limitations, it is expected that if the iodine emission fluxes are driven by the same processes, this should be correctly reflected by the trend of the calculated fluxes. However, especially close to the Indian subcontinent, opposite trends between the calculated fluxes for I_2 and HOI and the observed IO concentrations are found. Indeed, at 12°N, the IO mixing ratios are smaller than at 8° N, although the HOI and I_2 fluxes are larger by a factor of almost 2. The highest daily averaged IO mixing ratio is observed at about 8.5°N. In order to explain this discrepancy, we look at the possible mechanisms that might cause lower atmospheric IO concentrations in the presence of a higher inorganic iodine flux from the ocean.

As mentioned, the main source of iodine compounds in the open ocean is in the form of inorganic iodine emissions (Mahajan, Plane, et al., 2010; Carpenter et al., 2013). Once the oceanic HOI and I_2 are equilibrated into the atmosphere through ocean-air interaction, they undergo photolysis to produce I atoms ((R3) and (R4)). The I atoms then react with O_3 to form IO (R5).

$$\mathrm{HOI} + h\upsilon \rightarrow \mathrm{I} + \mathrm{OH} \qquad \text{(Bauer et al., 1998)} \qquad \text{(R3)}$$

$$\mathrm{I_2} + h\upsilon \rightarrow 2\mathrm{I} \qquad \text{(Saiz-Lopez et al., 2004)} \qquad \text{(R4)}$$

$$\mathrm{I} + \mathrm{O_3} \rightarrow \mathrm{IO} + \mathrm{O_2} \quad k(298\ \mathrm{K}) = 1.3\times10^{-12}\ \mathrm{cm^3\cdot molecule^{-1}\cdot s^{-1}} \qquad \text{(Atkinson et al., 2007)} \qquad \text{(R5)}$$

IO can undergo several different reactions in order to form higher iodine oxides, HOI, or recycle back to I (Sommariva et al., 2012). However, in the presence of NO_2, it can also lead to the formation of $IONO_2$ (R6), which can act as a reservoir species for iodine.

$$IO + NO_2 + M \rightarrow IONO_2 + M \quad k(298\ K) = 3.48\times10^{-12}\ cm^3\cdot molecule^{-1}\cdot s^{-1} \text{ at 1 bar} \qquad \text{(Atkinson et al., 2007)} \quad (R6)$$

The resulting $IONO_2$ can photolyze (2×10^{-3} s^{-1}, for clear-sky conditions in the tropics; Mössinger et al., 2002) or undergo thermal decomposition back to IO + NO_2 (3.5×10^{-5} s^{-1} at 298 K; Atkinson et al., 2007). For these two processes to dominate over the formation of $IONO_2$, NO_2 has to be below ~100 pptv, which is observed in the remote open ocean environment but not close to the Indian subcontinent where anthropogenic emissions result in larger levels of NO_2. $IONO_2$ can also react with I atoms to recycle back to I_2 (5.6×10^{-11} $cm^2\cdot molecule^{-1}\cdot s^{-1}$ at 298 K; Kaltsoyannis & Plane, 2008), as has been observed in semipolluted environments (Mahajan et al., 2009). However, for this to occur, a substantial concentration of I atoms and a $[IONO_2]/[O_3]$ ratio greater than 0.01 is required (Kaltsoyannis & Plane, 2008). At the low concentrations of IO observed during IIOE-2, the concentrations of I atoms are too low (0.12 pptv) for the reverse reaction to play an important role and, as pointed out above, nor does the photolysis and thermal decomposition compete with the formation of $IONO_2$. The lifetime for heterogeneous recycling of $IONO_2$ through aerosol uptake, considering an upper limit aerosol surface area of 1×10^{-6} cm^2/cm^3 and an uptake coefficient of 0.1, is about 0.6 hr, which is too slow in comparison with its formation rate at $NO_2 > 100$ pptv. Hence, in the presence of elevated NO_2, the IO will get titrated to the reservoir species $IONO_2$, leading to values lower than the detection limit of the MAX-DOAS instrument.

During IIOE-2, as mentioned above, the NO_2 DSCDs were observed above the detection limit of the instrument only close to the Indian subcontinent. The peak mixing ratio of 854 ± 223 pptv was also observed close to the Indian subcontinent. Additionally, the monthly mean satellite data for December 2015 in Figure 5d shows the southward latitudinal reduction in the tropospheric NO_2 VCDs. Peak column densities between 1.6×10^{15} and 1.8×10^{15} molecules·cm^{-2} are observed on 4 December (15°N), with a significant reduction along the cruise track away from the Indian coast. The backtrajectories also show that the air masses passing over the Indian subcontinent were sampled until 7 December (10°N), after which the wind pattern changes and air masses are mostly oceanic in origin. The oceanic air masses should have lower levels of NO_2 due to the lack of anthropogenic emissions, which is reflected in the tropospheric column densities and the surface-based MAX-DOAS observations (MAX-DOAS detection limit is ~120 pptv). At low NO_2 concentrations, the IO is not titrated and hence is observed above the detection limit of the instrument. At present, global models overestimate the concentrations of IO close to the Indian subcontinent. A Goddard Earth Observing System - Chemistry (GEOS-Chem)-based study by Sherwen, Evans, et al. (2016) has reported upward of 1 pptv close to the Indian coast, which is much larger than the observed levels. The Community Atmosphere Model with Chemistry (CAM-Chem) model is closer to the observations but still shows more than 0.5 pptv close to the Indian subcontinent (Prados-Roman et al., 2015; Saiz-Lopez et al., 2014). It should be noted that the models reproduce well the open ocean observations although GEOS-Chem overpredicts the IO concentrations in the Indian Ocean.

In the remote open ocean environment, the distribution of IO tracks the trend of the estimated HOI and I_2 fluxes, with lower atmospheric IO as the cruise progressed toward the Mauritius. Indeed, the IO mixing ratios were close to or below the detection toward the end of the study period, when the HOI and I_2 fluxes were at their lowest. In view of observations in the Pacific (Gómez Martín et al., 2013; Mahajan et al., 2012), it could be argued that the trends of IO observed in this study can be explained by a shift in the partitioning of reactive iodine speciation. Values around 1 pptv for IO + I have been reported in the eastern Pacific MBL, with the IO:I ratio about 2:1, with IO mixing ratios around 0.6 pptv (Mahajan et al., 2012). We checked whether the change in ozone from above 20 to 10 ppbv can explain the trend of IO rather than the change in the fluxes. The calculated IO + I peaks at 0.58 ± 0.31 pptv in the Northern Hemisphere outside the high-NO_x regions and followed a similar trend to the IO observations, although with a smaller gradient, reducing to 0.35 ± 0.28 pptv below the equator. This suggests that the iodide calculated using parameterization reported by Chance et al. (2014) and the parameterizations for the fluxes by Carpenter et al. (2013) are able to capture the geographical variation of atmospheric IO, in regions of low NO_x. Comparison with past observations of iodide and IO around the world suggests that the second parameterization equation (equation (2)) overestimates the iodide concentration and resultant fluxes in the Indian Ocean. Additionally, in regions with elevated NO_x, the atmospheric IO is controlled by titration reaction rather than the flux of inorganic

species (Mahajan et al., 2009; Platt & Janssen, 1995). This would reduce the impact of iodine chemistry on ozone destruction closer to the Indian subcontinent and needs to be accurately calculated in large-scale models.

4. Conclusions

Here we report measurements of atmospheric IO during the IIOE-2 in addition to oceanic observations of SST, salinity, MLD_{pt}, and nitrate concentrations. The oceanic parameters were used to calculate the predicted seawater iodide concentrations, and the resultant HOI and I_2 fluxes from the ocean to the atmosphere. The estimated fluxes for inorganic iodine compounds were several times larger close to the Indian subcontinent in the Arabian Sea as compared with the remote open ocean environment. However, the atmospheric IO mixing ratios were lower close to the Indian subcontinent. It is suggested that this discrepancy is due to titration of IO by NO_2, which is corroborated by the MAX-DOAS and satellite-based NO_2 observations. In the remote ocean MBL, the atmospheric IO tracks the estimated HOI and I_2 fluxes, adding weight to the reports that oceanic inorganic iodine emissions are the main source for iodine in the remote open ocean MBL. Finally, these observations show that the flux estimates for HOI and I_2 can explain the atmospheric distribution of IO in the Indian Ocean, but a correlation between the fluxes and atmospheric IO is observable only in the low-NO_x regions as NO_x-based titration dominates in areas with elevated NO*x*.

Acknowledgments
IITM and NCAOR are funded by the Ministry of Earth Sciences, Government of India. The first IIOE-2 expedition was supported by ESSO-INCOIS. We thank the Captain, staff, and crew of ORV *Sagar Nidhi* for their cooperation and support. P. N. V. acknowledges partial support from the HOOFS program of INCOIS. LT, RC and LJC thank the UK Natural Environment Research Council (NERC) for funding (Grant no. NE/N009983/1). All the data used are listed in the references or archived in the ResearchGate repository (https://www.researchgate.net/profile/Anoop_Mahajan/publication/325415099_This_data_is_all_a_part_of_the_a_publication_on_Understanding_iodine_chemistry_during_the_2nd_International_Indian_Ocean_Expedition_IIOE-2/data/5b0ce1630f7e9b1ed7fbcd51/data.rar).

References

Alicke, B., Hebestreit, K., Stutz, J., & Platt, U. (1999). Iodine oxide in the marine boundary layer. *Nature*, *397*(6720), 572–573. https://doi.org/10.1038/17508

Allan, B., McFiggans, G., Plane, J. M. C., & Coe, H. (2000). Observations of iodine monoxide in the remote marine boundary layer. *Journal of Geophysics*, *105*(D11), 14,363–14,369. https://doi.org/10.1029/1999JD901188

Atkinson, R., Baulch, D. L., Cox, R. A., Crowley, J. N., Hampson, R. F., Hynes, R. G., et al. (2007). Evaluated kinetic and photochemical data for atmospheric chemistry: Volume III—Gas phase reactions of inorganic halogens. *Atmospheric Chemistry and Physics*, *7*(4), 981–1191. https://doi.org/10.5194/acp-7-981-2007

Bauer, D., Ingham, T., Carl, S. A., Moortgat, G. K., & Crowley, J. N. (1998). Ultraviolet-visible absorption cross sections of gaseous HOI and its photolysis at 355 nm. *The Journal of Physical Chemistry. A*, *102*, 2857–e2864.

Boersma, K. F. (2004). Error analysis for tropospheric NO_2 retrieval from space. *Journal of Geophysical Research*, *109*, D04311. https://doi.org/10.1029/2003JD003962

Boersma, K. F., Eskes, H. J., Veefkind, J. P., Brinksma, E. J., Sneep, M., Levelt, P. F., et al. (2007). Near-real time retrieval of tropospheric NO_2 from OMI. *Atmospheric Chemistry and Physics*, *7*(8), 2103–2118. https://doi.org/10.5194/acp-7-2103-2007

Bogumil, K., Orphal, J., Homann, T., Voigt, S., Spietz, P., Fleischmann, O. C., et al. (2003). Measurements of molecular absorption spectra with the SCIAMACHY pre-flight model: Instrument characterization and reference data for atmospheric remote-sensing in the 230–2380 nm region. *Journal of Photochemistry and Photobiology A: Chemistry*, *157*(2–3), 167–184. https://doi.org/10.1016/S1010-6030(03)00062-5

Burkill, P. H., Mantoura, R. F. C., & Owens, N. J. (1993). Biogeochemical cycling in the northwestern Indian Ocean: A brief overview. *Deep-Sea Research Part II: Topical Studies in Oceanography*, *40*(3), 643–649. https://doi.org/10.1016/0967-0645(93)90049-S

Carpenter, L., & Nightingale, P. D. (2015). Chemistry and release of gases from the Surface Ocean. *Chemical Reviews*, *115*(10), 4015–4034. https://doi.org/10.1021/cr5007123

Carpenter, L. J. (2003). Iodine in the marine boundary layer. *Chemical Reviews*, *103*(12), 4953–4962. https://doi.org/10.1021/Cr0206465

Carpenter, L. J., MacDonald, S. M., Shaw, M. D., Kumar, R., Saunders, R. W., Parthipan, R., et al. (2013). Atmospheric iodine levels influenced by sea surface emissions of inorganic iodine. *Nature Geoscience*, *6*(2), 108–111. https://doi.org/10.1038/ngeo1687

Chameides, W. L., & Davis, D. D. (1980). Iodine: Its possible role in tropospheric photochemistry. *Journal of Geophysical Research*, *85*(C12), 7383–7398. https://doi.org/10.1029/JC085iC12p07383

Chance, K. V., & Spurr, R. J. (1997). Ring effect studies: Rayleigh scattering, including molecular parameters for rotational Raman scattering, and the Fraunhofer spectrum. *Applied Optics*, *36*(21), 5224–5230.

Chance, R., Baker, A. R., Carpenter, L., & Jickells, T. D. (2014). The distribution of iodide at the sea surface. *Environmental Science: Processes & Impacts*, *16*(8), 1841–1859. https://doi.org/10.1039/c4em00139g

Commane, R., Seitz, K., Bale, C. S. E., Bloss, W. J., Buxmann, J., Ingham, T., et al. (2011). Iodine monoxide at a clean marine coastal site: Observations of high frequency variations and inhomogeneous distributions. *Atmospheric Chemistry and Physics*, *11*(13), 6721–6733. https://doi.org/10.5194/acp-11-6721-2011

Cullen, J. J., Franks, P. J., Karl, D. M., & Longhurst, A. (2002). Physical influences on marine ecosystem dynamics. In A. R. Robinson, J. J. McCarthy, & B. J. Rothschild (Eds.), *The Sea* (pp. 297–336). New York: John Wiley.

Dileepkumar, M. (2006). Biogeochemistry of the North Indian Ocean, in IGBP-WCRP-SCOPE Report Series 1.

Dinter, T., Rozanov, V. V., Burrows, J. P., & Bracher, A. (2015). Retrieving the availability of light in the ocean utilising spectral signatures of vibrational Raman scattering in hyper-spectral satellite measurements. *Ocean Science*, *11*(3), 373–389. https://doi.org/10.5194/os-11-373-2015

Dix, B., Baidar, S., Bresch, J. F., Hall, S. R., Schmidt, K. S., Wang, S., & Volkamer, R. (2013). Detection of iodine monoxide in the tropical free troposphere. *Proceedings of the National Academy of Sciences of the United States of America*, *110*(6), 2035–2040. https://doi.org/10.1073/pnas.1212386110

D'Ortenzio, F., Lavigne, H., Besson, F., Claustre, H., Coppola, L., Garcia, N., et al. (2014). Observing mixed layer depth, nitrate and chlorophyll concentrations in the northwestern Mediterranean: A combined satellite and NO_3 profiling floats experiment. *Geophysical Research Letters*, *41*, 6443–6451. https://doi.org/10.1002/2014GL061020

Draxler, R., & Rolph, G. (2003). HYSPLIT (HYbrid Single Particle Lagrangian Integrated Trajectory). Model access via NOAA ARL Ready. Retrieved from http://www.arl.noaa.gov/ready/hysplit4.html

Dutkiewicz, S., Follows, M., Marshall, J., & Gregg, W. (2001). Interannual variability of phytoplankton abundances in the North Atlantic. *Deep-Sea Research Part II: Topical Studies in Oceanography*, *48*(10), 2323–2344. https://doi.org/10.1016/S0967-0645(00)00178-8

Farrenkopf, A. M., & Luther, G. W. (2002). Iodine chemistry reflects productivity and denitrification in the Arabian Sea: Evidence for flux of dissolved species from sediments of western India into the OMZ. *Deep Sea Research Part II: Topical Studies in Oceanography*, *49*(12), 2303–2318. https://doi.org/10.1016/S0967-0645(02)00038-3

Fayt, C., & Van Roozendael, M. (2013). QDOAS 1.00. Software user manual. Retrieved from http://uv-vis.aeronomie.be/software/QDOAS/

Frieß, U., Wagner, T., Pundt, I., Pfeilsticker, K., Platt, U., & Friefi, U. (2001). Spectroscopic measurements of tropospheric iodine oxide at Neumayer Station, Antarctica. *Geophysical Research Letters*, *28*(10), 1941–1944. https://doi.org/10.1029/2000GL012784

Ganzeveld, L. (2009). Atmosphere-ocean ozone exchange: A global modelling study of biogechemical, atmospheric and waterside turbulence dependencies. *Global Biogeochemical Cycles*, *23*, GB4021. https://doi.org/10.1029/2008GB003301

Garland, J. A., & Curtis, H. (1981). Emission of iodine from the sea surface in the presence of ozone. *Journal of Geophysical Research*, *86*(C4), 3183–3186. https://doi.org/10.1029/JC086iC04p03183

Gómez Martín, J. C., Mahajan, A. S., Hay, T. D., Prados-Román, C., Ordóñez, C., MacDonald, S. M., et al. (2013). Iodine chemistry in the eastern Pacific marine boundary layer. *Journal of Geophysical Research: Atmospheres*, *118*, 887–904. https://doi.org/10.1002/jgrd.50132

Gómez Martín, J. C., Spietz, P., & Burrows, J. P. (2005). Spectroscopic studies of the I_2/O_3 photochemistry—Part 1: Determination of the absolute absorption cross sections of iodine oxides of atmospheric relevance. *Journal of Photochemistry and Photobiology A: Chemistry*, *176*(1–3), 15–38. https://doi.org/10.1016/j.jphotochem.2005.09.024

Gómez Martín, J. C., Vömel, H., Hay, T. D., Mahajan, A. S., Ordóñez, C., Parrondo Sempere, M. C., et al. (2016). On the Variability of Ozone in the Equatorial Eastern Pacific Boundary Layer. *Journal of Geophysical Research: Atmospheres*, *120*(1), 199–214. https://doi.org/10.1002/2014JD022310

Greenblatt, G. D., Orlando, J. J., Burkholder, J. B., & Ravishankara, A. R. (1990). Absorption measurements of oxygen between 330 and 1140 nm. *Journal of Geophysical Research*, *95*(D11), 18,577–18,582. https://doi.org/10.1029/JD095iD11p18577

Großmann, K., Frieß, U., Peters, E., Wittrock, F., Lampel, J., Yilmaz, S., et al. (2013). Iodine monoxide in the Western Pacific marine boundary layer. *Atmospheric Chemistry and Physics*, *13*(6), 3363–3378. https://doi.org/10.5194/acp-13-3363-2013

Hausmann, M., & Platt, U. (1994). Spectroscopic measurement of bromine oxide and ozone in the high arctic during Polar Sunrise Experiment 1992. *Journal of Geophysical Research*, *99*(D12), 25,399–25,413. https://doi.org/10.1029/94JD01314

Hayase, S., Yabushita, A., Kawasaki, M., Enami, S., Hoffmann, M. R., & Colussi, A. J. (2010). Heterogenous reactions of gaseous ozone with aqueous iodide in the presence of aqueous organic species. *The Journal of Physical Chemistry. A*, *114*(19), 6016–6021. https://doi.org/10.1021/jp101985f

Hepach, H., Quack, B., Tegtmeier, S., Engel, A., Bracher, A., Fuhlbrügge, S., et al. (2016). Biogenic halocarbons from the Peruvian upwelling region as tropospheric halogen source. *Atmospheric Chemistry and Physics*, *16*(18), 12,219–12,237. https://doi.org/10.5194/acp-16-12219-2016

Hönninger, G., von Friedeburg, C., & Platt, U. (2004). Multi axis differential optical absorption spectroscopy (MAX-DOAS). *Atmospheric Chemistry and Physics*, *4*(1), 231–254. https://doi.org/10.5194/acp-4-231-2004

Intergovernmental Oceanographic Commission (2010). Manuals and guides no. 56. The international thermodynamic equation of seawater: Calculation and use of thermodynamic properties.

Jimenez, J. L. (2003). New particle formation from photooxidation of diiodomethane (CH_2I_2). *Journal of Geophysical Research*, *108*(D10), 4318. https://doi.org/10.1029/2002JD002452

Johnson, K. S., Riser, S. C., & Karl, D. M. (2010). Nitrate supply from deep to near-surface waters of the North Pacific subtropical gyre. *Nature*, *465*(7301), 1062–1065. https://doi.org/10.1038/nature09170

Kaltsoyannis, N., & Plane, J. M. C. (2008). Quantum chemical calculations on a selection of iodine-containing species (IO, OIO, INO_3, $(IO)_2$, I_2O_3, I_2O_4 and I_2O_5) of importance in the atmosphere. *Physical Chemistry Chemical Physics*, *10*(13), 1723–1733. https://doi.org/10.1039/b715687c

Kumar, K. K., Rajagopalan, B., Hoerling, M., Bates, G., & Cane, M. (2006). Unraveling the mystery of Indian monsoon failure during El Niño. *Science*, *314*(5796), 115–119.

Kurucz, R.L., Furenlid, I., Brault, J., Testerman, L. (1984). Solar flux atlas from 296 to 1300 nm. Technical report, *National Solar Observatory*.

Lampel, J., Pöhler, D., Tschritter, J., Frieß, U., & Platt, U. (2015). On the relative absorption strengths of water vapour in the blue wavelength range. *Atmospheric Measurement Techniques*, *8*(10), 4329–4346. https://doi.org/10.5194/amt-8-4329-2015

Liss, P. S., & Slater, P. G. (1974). Flux of gases across air-sea interface. *Nature*, *247*(5438), 181–184. https://doi.org/10.1038/247181a0

MacDonald, S. M., Gómez Martín, J. C., Chance, R., Warriner, S., Saiz-Lopez, A., Carpenter, L. J., & Plane, J. M. C. (2014). A laboratory characterisation of inorganic iodine emissions from the sea surface: Dependence on oceanic variables and parameterisation for global modelling. *Atmospheric Chemistry and Physics*, *14*(11), 5841–5852. https://doi.org/10.5194/acp-14-5841-2014

Mahajan, A. S., Gómez Martín, J. C., Hay, T. D., Royer, S. J., Yvon-Lewis, S., Liu, Y., et al. (2012). Latitudinal distribution of reactive iodine in the eastern Pacific and its link to open ocean sources. *Atmospheric Chemistry and Physics*, *12*(23), 11,609–11,617. https://doi.org/10.5194/acp-12-11609-2012

Mahajan, A. S., Oetjen, H., Saiz-Lopez, A., Lee, J. D., McFiggans, G. B., & Plane, J. M. C. (2009). Reactive iodine species in a semi-polluted environment. *Geophysical Research Letters*, *36*, L16803. https://doi.org/10.1029/2009GL038018

Mahajan, A. S., Plane, J. M. C., Oetjen, H., Mendes, L. M., Saunders, R. W., Saiz-Lopez, A., et al. (2010). Measurement and modelling of tropospheric reactive halogen species over the tropical Atlantic Ocean. *Atmospheric Chemistry and Physics*, *10*(10), 4611–4624. https://doi.org/10.5194/acp-10-4611-2010

Mahajan, A. S., Shaw, M., Oetjen, H., Hornsby, K. E., Carpenter, L. J., Kaleschke, L., et al. (2010). Evidence of reactive iodine chemistry in the Arctic boundary layer. *Journal of Geophysical Research*, *115*, D20303. https://doi.org/10.1029/2009JD013665

Mann, K. H., & Lazier, J. R. N. (1996). *Dynamics of marine ecosystems: Biological-physical interactions in the oceans*. New York: Blackwell Publishing.

McConnell, J. C., Henderson, G. S., Barrie, L. A., Bottenheim, J. W., Niki, H., Landford, C. H., & Templeton, E. M. J. (1992). Photochemical bromine production implicated in arctic boundary layer ozone depletion. *Nature*, *355*(6356), 150–152. https://doi.org/10.1038/355150a0

McFiggans, G. B., Bale, C. S. E., Ball, S. M., Beames, J. M., Bloss, W. J., Carpenter, L. J., et al. (2010). Iodine-mediated coastal particle formation: An overview of the Reactive Halogens in the Marine Boundary Layer (RHaMBLe) Roscoff coastal study. *Atmospheric Chemistry and Physics*, *10*(6), 2975–2999. https://doi.org/10.5194/acp-10-2975-2010

McFiggans, G. B., Coe, H., Burgess, R., Allan, J., Cubison, M., Alfarra, M. R., et al. (2004). Direct evidence for coastal iodine particles from Laminaria macroalgae—Linkage to emissions of molecular iodine. *Atmospheric Chemistry and Physics*, *4*(3), 701–713. https://doi.org/10.5194/acp-4-701-2004

Meller, R., & Moortgat, G. K. (2000). Temperature dependence of the absorption cross sections of formaldehyde between 223 and 323 K in the wavelength range 225–375 nm. *Journal of Geophysical Research*, *105*(D6), 7089–7101. https://doi.org/10.1029/1999JD901074

Miyake, Y., & Tsunogai, S. (1963). Evaporation of iodine from ocean. *Journal of Geophysical Research*, *68*(13), 3989–3993. https://doi.org/10.1029/JZ068i013p03989

Monterey, G., & Levitus, S. (1997). *Seasonal variability of mixed layer depth for the World Ocean*. Washington, D.C.: U.S. Government Printing Office.

Mössinger, J. C., Rowley, D. M., & Cox, R. A. (2002). The UV-visible absorption cross-sections of $IONO_2$. *Atmospheric Chemistry and Physics*, *2*(3), 227–234. https://doi.org/10.5194/acp-2-227-2002

Narvekar, J., & Prasanna Kumar, S. (2006). Seasonal variability of the mixed layer in the central Bay of Bengal and associated changes in nutrients and chlorophyll. *Deep Sea Research Part I: Oceanographic Research Papers*, *53*(5), 820–835. https://doi.org/10.1016/j.dsr.2006.01.012

O'Dowd, C. D., Facchini, M. C., Cavalli, F., Ceburnis, D., Mircea, M., Decesari, S., et al. (2004). Biogenically driven organic contribution to marine aerosol. *Nature*, *431*(7009), 676–680. https://doi.org/10.1038/nature02970.1

O'Dowd, C. D., Jimenez, J. L., Bahreini, R., Flagan, R. C., Seinfeld, J. H., Hämeri, K., et al. (2002). Marine aerosol formation from biogenic iodine emissions. *Nature*, *417*(6889), 632–636. https://doi.org/10.1038/nature00773.1.2.3.4.5.6.7.8.9.10

Oetjen, H. (2009). Measurements of halogen oxides by scattered sunlight differential optical absorption spectroscopy, University of Bremen.

Peters, E., Wittrock, F., Richter, A., Alvarado, L. M. A., Rozanov, V. V., & Burrows, J. P. (2014). Liquid water absorption and scattering effects in DOAS retrievals over oceans. *Atmospheric Measurement Techniques*, *7*(12), 4203–4221. https://doi.org/10.5194/amt-7-4203-2014

Plane, J. M. C., & Saiz-Lopez, A. (2006). UV-visible differential optical absorption spectroscopy (DOAS). In D. E. Heard (Ed.), *Analytical techniques for atmospheric measurement* (pp. 147–188). Oxford, UK: Wiley-Blackwell.

Platt, U., & Janssen, C. (1995). Observation and role of the free radicals NO_3 C1O, BrO and IO in the troposphere. *Faraday Discussions*, *100*, 175. https://doi.org/10.1039/fd9950000175

Platt, U., & Stutz, J. (2008). *Differential optical absorption spectroscopy: Principles and applications*, (1st ed.). Berlin Heidelberg: Springer.

Pope, R. M., & Fry, E. S. (1997). Absorption spectrum (380–700 nm) of pure water. II. Integrating cavity measurements. *Applied Optics*, *36*(33), 8710–8723.

Prados-Roman, C., Cuevas, C. A., Hay, T., Fernandez, R. P., Mahajan, A. S., Royer, S. J., et al. (2015). Iodine oxide in the global marine boundary layer. *Atmospheric Chemistry and Physics*, *15*(2), 583–593. https://doi.org/10.5194/acp-15-583-2015

Prasanna Kumar, S., & Narvekar, J. (2005). Seasonal variability of the mixed layer in the central Arabian Sea and its implication on nutrients and primary productivity. *Deep Sea Research Part II: Topical Studies in Oceanography*, *52*(14-15), 1848–1861. https://doi.org/10.1016/j.dsr2.2005.06.002

Puentedura, O., Gil, M., Saiz-Lopez, A., Hay, T., Navarro-Comas, M., Gómez-Pelaez, A., et al. (2002). Iodine monoxide in the north subtropical free troposphere. *Atmospheric Chemistry and Physics*, *12*, 4909–4921. https://doi.org/10.5194/acp-12-4909-2012

Read, K. A., Mahajan, A. S., Carpenter, L. J., Evans, M. J., Faria, B. V. E., Heard, D. E., et al. (2008). Extensive halogen-mediated ozone destruction over the tropical Atlantic Ocean. *Nature*, *453*(7199), 1232–1235. https://doi.org/10.1038/nature07035

Rothman, L. S., Gordon, I. E., Babikov, Y., Barbe, A., Chris Benner, D., Bernath, P. F., et al. (2013). The HITRAN 2012 molecular spectroscopic database. *Journal of Quantitative Spectroscopy and Radiation Transfer*, *130*, 4–50. https://doi.org/10.1016/j.jqsrt.2013.07.002

Roxy, M. K., Ritika, K., Terray, P., & Masson, S. (2014). The curious case of Indian Ocean warming. *Journal of Climate*, *27*(22), 8501–8509. https://doi.org/10.1175/JCLI-D-14-00471.1

Sadeghi, A., Dinter, T., Vountas, M., Taylor, B. B., Altenburg-Soppa, M., Peeken, I., & Bracher, A. (2012). Improvement to the phytodoas method for identification of coccolithophores using hyper-spectral satellite data. *Ocean Science*, *8*(6), 1055–1070. https://doi.org/10.5194/os-8-1055-2012

Saiz-Lopez, A., Chance, K. V., Liu, X., Kurosu, T. P., & Sander, S. P. (2007). First observations of iodine oxide from space. *Geophysical Research Letters*, *34*, L12812. https://doi.org/10.1029/2007GL030111

Saiz-Lopez, A., Fernandez, R. P., Ordóñez, C., Kinnison, D. E., Gómez Martín, J. C., Lamarque, J.- F., & Tilmes, S. (2014). Iodine chemistry in the troposphere and its effect on ozone. *Atmospheric Chemistry and Physics*, *14*(23), 13,119–13,143. https://doi.org/10.5194/acp-14-13119-2014

Saiz-Lopez, A., Lamarque, J. F., Kinnison, D. E., Tilmes, S., Ordóñez, C., Orlando, J. J., et al. (2012). Estimating the climate significance of halogen-driven ozone loss in the tropical marine troposphere. *Atmospheric Chemistry and Physics*, *12*(9), 3939–3949. https://doi.org/10.5194/acp-12-3939-2012

Saiz-Lopez, A., Mahajan, A. S., Salmon, R. A., Bauguitte, S. J.-B., Jones, A. E., Roscoe, H. K., & Plane, J. M. C. (2007). Boundary layer halogens in coastal Antarctica. *Science*, *317*(5836), 348–351. https://doi.org/10.1126/science.1141408

Saiz-Lopez, A., & Plane, J. M. C. (2004). Novel iodine chemistry in the marine boundary layer. *Geophysical Research Letters*, *31*, L04112. https://doi.org/10.1029/2003GL019215

Saiz-Lopez, A., Plane, J. M. C., Baker, A. R., Carpenter, L. J., von Glasow, R., Martín, J. C. G., et al. (2012). Atmospheric chemistry of iodine. *Chemical Reviews*, *112*(3), 1773–1804. https://doi.org/10.1021/cr200029u

Saiz-Lopez, A., Plane, J. M. C., McFiggans, G. B., Williams, P. I., Ball, S. M., Bitter, M., et al. (2006). Modelling molecular iodine emissions in a coastal marine environment: The link to new particle formation. *Atmospheric Chemistry and Physics*, *6*(4), 883–895. https://doi.org/10.5194/acp-6-883-2006

Saiz-Lopez, A., Saunders, R. W., Joseph, D. M., Ashworth, S. H., & Plane, J. M. C. (2004). Absolute absorption cross-section and photolysis rate of I_2. *Atmospheric Chemistry and Physics*, *4*(5), 1443–1450. https://doi.org/10.5194/acp-4-1443-2004

Saiz-Lopez, A., & von Glasow, R. (2012). Reactive halogen chemistry in the troposphere. *Chemical Society Reviews*, *41*(19), 6448. https://doi.org/10.1039/c2cs35208g

Saji, N. H., Goswami, B. N., Vinayachandran, P. N., & Yamagata, T. (1999). A dipole mode in the tropical Indian Ocean. *Nature*, *401*(6751), 360–363. https://doi.org/10.1038/43854

Sakamoto, Y., Yabushita, A., Kawasaki, M., & Enami, S. (2009). Direct emission of I_2 molecule and IO radical from the heterogeneous reactions of gaseous ozone with aqueous potassium iodide solution. *The Journal of Physical Chemistry. A*, *113*(27), 7707–7713. https://doi.org/10.1021/jp903486u

Schönhardt, A., Richter, A., Wittrock, F., Kirk, H., Oetjen, H., Roscoe, H. K., & Burrows, J. P. (2008). Observations of iodine monoxide (IO) columns from satellite. *Atmospheric Chemistry and Physics*, *8*(3), 637–653. https://doi.org/10.5194/acp-8-637-2008

Schroeder, W. H., Anlauf, K. G., Barrie, L. A., Lu, J. Y., Steffen, A., Schneeberger, D. R., & Berg, T. (1998). Arctic springtime deleption of mercury. *Nature*, *394*(6691), 331–332. https://doi.org/10.1038/28530

Seinfeld, J. H., & Pandis, S. N. (2006). *Atmospheric chemistry and physics: From air pollution to climate change*, (2nd ed.). New York: John Wiley & Sons.

Sherwen, T., Evans, M. J., Carpenter, L. J., Andrews, S. J., Lidster, R. T., Dix, B., et al. (2016). Iodine's impact on tropospheric oxidants: A global model study in GEOS-Chem. *Atmospheric Chemistry and Physics*, *16*(2), 1161–1186. https://doi.org/10.5194/acp-16-1161-2016

Sherwen, T., Evans, M. J., Carpenter, L. J., Schmidt, J. A., & Mickely, L. J. (2017). Halogen chemistry reduces tropospheric O3 radiative forcing. *Atmospheric Chemistry and Physics*, *17*(2), 1557–1569. https://doi.org/10.5194/acp-17-1557-2017

Sherwen, T., Schmidt, J. A., Evans, M. J., Carpenter, L. J., Großmann, K., Eastham, S. D., et al. (2016). Global impacts of tropospheric halogens (Cl, Br, I) on oxidants and composition in GEOS-Chem. *Atmospheric Chemistry and Physics*, *16*, 1–52. https://doi.org/10.5194/acp-2016-424.

Sinreich, R., Coburn, S., Dix, B., & Volkamer, R. (2010). Ship-based detection of glyoxal over the remote tropical Pacific Ocean. *Atmospheric Chemistry and Physics*, *10*(23), 11,359–11,371. https://doi.org/10.5194/acp-10-11359-2010

Sommariva, R., Bloss, W. J., & von Glasow, R. (2012). Uncertainties in gas-phase atmospheric iodine chemistry. *Atmospheric Environment*, *57*, 219–232. https://doi.org/10.1016/j.atmosenv.2012.04.032

Truesdale, V. W. (1978). Iodine in inshore and off-shore marine waters. *Marine Chemistry*, *6*(1), 1–13. https://doi.org/10.1016/0304-4203(78)90002-6

Vandaele, A. C., Hermans, C., Simon, P., Carleer, M. R., Colins, R., Fally, F., et al. (1997). Measurements of NO_2 absorption cross-sections at 42000 cm^{-1} to 10000 cm^{-1} (238-1000 nm) at 220 K and 298 K. *Journal of Quantitative Spectroscopy and Radiation Transfer*, *59*, 171–184.

Volkamer, R. A., Spietz, P., Burrows, J. P., & Platt, U. (2005). High-resolution absorption cross-section of glyoxal in the UV-vis and IR spectral ranges. *Journal of Photochemistry and Photobiology A: Chemistry*, *172*(1), 35–46. https://doi.org/10.1016/j.jphotochem.2004.11.011

Vountas, M., Dinter, T., Bracher, A., Burrows, J., & Sierk, B. (2007). Spectral studies of ocean water with space-borne sensor SCIAMACHY using differential optical absorption spectroscopy (DOAS). *Ocean Science*, *3*(3), 429–440. https://doi.org/10.5194/os-3-429-2007

Wagner, T., Beirle, S., & Deutschmann, T. (2009). Three-dimensional simulation of the Ring effect in observations of scattered sun light using Monte Carlo radiative transfer models. *Atmospheric Measurement Techniques*, *2*(1), 113–124. https://doi.org/10.5194/amt-2-113-2009

Wagner, T., Dix, B., Friedeburg, C. V., Frieß, U., Sanghavi, S., Sinreich, R., & Platt, U. (2004). MAX-DOAS O_4 measurements: A new technique to derive information on atmospheric aerosols—Principles and information content. *Journal of Geophysical Research*, *109*, D22205. https://doi.org/10.1029/2004JD004904

Wiggert, J. D., Hood, R. R., Naqvi, S. W. A., Brink, K. H., & Smith, S. L. (2009). Introduction to Indian Ocean biogeochemical processes and ecological variability: Current understanding and emerging perspectives. In J. D. Wiggert, R. R. Hood, S. Wajih, A. Naqvi, K. H. Brink, & S. L. Smith (Eds.), *Indian Ocean Biogeochemical Processes and Ecological Variability* (pp. 1–9). Washington, DC: American Geophysical Union.

Wilmouth, D. M., Hanisco, T. F., Donahue, N. M., & Anderson, J. G. (1999). Fourier transform ultraviolet spectroscopy of the A $^2\Pi 3/2 \leftarrow$ X $^2\Pi 3/2$ transition of BrO. *The Journal of Physical Chemistry. A*, *103*(45), 8935–8945. https://doi.org/10.1021/jp991651o